Inorganic Chemistry

Article

pubs.acs.org/IC

Sulfur Dioxide Activation: A Theoretical Investigation into Dual S═O Bond Cleavage by Three-Coordinate Molybdenum(III) Complexes

Robert Robinson, Jr.,[†] Kiana Khadem Abbasi,[‡] Alireza Ariafard,*[,†,‡] Robert Stranger,[§] and Brian F. Yates*[,†]

[†]School of Physical Sciences - Chemistry, University of Tasmania, Private Bag 75, Hobart TAS 7001, Australia

[‡]Department of Chemistry, Faulty of Science, Central Tehran Branch, Islamic Azad University, Shahrak Gharb, Tehran, Iran

[§]Research School of Chemistry, Australian National University, Canberra, ACT 0200, Australia

Supporting Information

ABSTRACT: Cummins et al. have observed that 3 equiv of $Mo(N[R]Ar)_3$ (R = $C(CD_3)_2CH_3$, Ar = 3,5-$C_6H_3Me_2$) are required for dual S═O bond cleavage within a SO_2 molecule. Using density functional theory calculations, this theoretical study investigates a mechanism for this SO_2 cleavage reaction that is mediated by MoL_3, where L = NH_2 or N[^{t}Bu]Ph. Our results indicate that an electron transfers into the SO_2 ligand, which leads to Mo oxidation and initiates SO_2 coordination along the quartet surface. The antiferromagnetic (AF) nature of the $(NH_2)_3Mo{-}SO_2$ adduct accelerates intersystem crossing onto the doublet surface. The first S═O bond cleavage occurs from the resulting doublet adduct and leads to formation of $L_3Mo{=}O$ and SO. Afterward, the released SO molecule is cleaved by the two remaining MoL_3, resulting in formation of $L_3Mo{=}S$ and an additional $L_3Mo{=}O$. This mononuclear mechanism is calculated to be strongly exothermic and proceeds via a small activation barrier, which is in accordance with experimental results. An additional investigation into a binuclear process for this SO_2 cleavage reaction was also evaluated. Our results show that the binuclear mechanism is less favorable than that of the mononuclear mechanism.

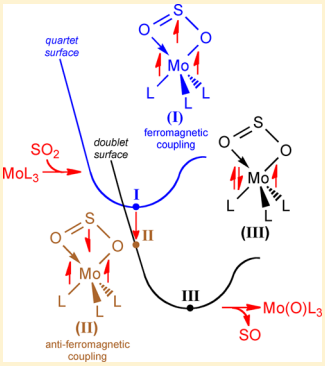

INTRODUCTION

Atmospheric pollution from SO_2 is a global concern due to its adverse effects on public health and on the environment alike. This hazardous pollutant is released into the atmosphere by sulfur-containing impurities in fossil fuels during combustion reaction processes. Strict desulfurization regulations by the Clean Air Act[1] to improve air quality have significantly reduced these SO_2 emissions. However, further emission reductions are still required to eliminate the severe threats from atmospheric SO_2. There are still practical limitations in adapting processes commercially for the complete removal of all sulfur impurities in fossil fuels that have encouraged new developments into more efficient technologies. To date, overcoming these limitations still remains fundamentally an important goal in environmental chemistry.[2,3] In the meantime, direct sulfur recovery processes (DSRPs), where SO_2 is reduced into elemental sulfur, have gained considerable attention as a means of transforming SO_2 into a prospective chemical feedstock. Earlier studies on SO_2 reactivity with various transition metal complexes predict that degradation of SO_2, such as occurs in DSRPs, can be a suitable route toward reducing SO_2 emissions.[4−6] In order to achieve this endeavor, a better understanding of SO_2 activation and S═O bond cleavage by transition metals is vital to assess the viability of this method.

Cummins et al. have reported the ability of $Mo(N[R]Ar)_3$ (R = $C(CD_3)_2CH_3$, Ar = 3,5-$C_6H_3Me_2$) to cleave bonds within various small molecules,[7−16] including both tri- and tetra-atomic species.[17,18] These experimental results on $Mo(N[R]Ar)_3$ have also been complemented by several theoretical studies in the literature.[19−26] Of significant importance is the reactivity of $Mo(N[R]Ar)_3$ toward a SO_2 molecule (eq 1).

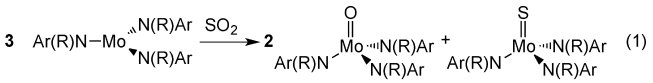

Ar = 3,5-$C_6H_3Me_2$; R = $C(CD_3)_2CH_3$

Initially, 1 equiv of $Mo(N[R]Ar)_3$ was reacted with SO_2, which produced the Mo-oxo complex, $(N[R]Ar)_3Mo(O)$ (confirmed by ^{2}H-NMR spectroscopy). However, the reaction of 3 equiv of $Mo(N[R]Ar)_3$ with SO_2 leads to the clean formation of 2 $(N[R]Ar)_3Mo(O)$ and the Mo-sulfido complex $(N[R]Ar)_3Mo(S)$. These outcomes demonstrate that $Mo(N[R]Ar)_3$ is not only effective at breaking the initial S═O bond but is also effective at the subsequent breaking of the second S═O bond.

Herein, a theoretical investigation into the mechanism by which 3 equiv of $Mo(N[R]Ar)_3$ interact with (activation) and fully dissociate (dual bond cleavage) a SO_2 molecule is discussed. We also provide the rationalization for how SO_2 is more reactive toward bond breaking reactions than other small molecules.

Received: September 22, 2014
Published: January 5, 2015

DOI: 10.1021/ic502298j
Inorg. Chem. 2015, 54, 534−543

COMPUTATIONAL DETAILS

Density functional theory (DFT) calculations were performed using the Gaussian 09[27] program package. Optimized geometries were located with the B3LYP[28−30] functional in the gas-phase and without symmetry constraints (298 K and 1 atm). The Stuttgart/Dresden double-ζ (SDD)[31] valence basis set with effective core potential (ECP) was used for Mo and the 6-31G(d)[32] basis set for all other atoms, referred to as BS1. At B3LYP/BS1, both minima with no imaginary frequency and transition structures with one imaginary frequency were confirmed with harmonic frequency calculations and vibrational mode analyses using the GaussView[33] program. Intrinsic reaction coordinate (IRC)[34,35] calculations were used to confirm the connectivity between minima and transition structures. Minimum energy crossing points (MECPs) between spin-states were located using the code of Harvey et al.[36] and are reported uncorrected due to the absence of stationary points. For better energy refinements, single-point energies (SPEs) were calculated using the B3LYP-D3BJ[37] and/or M06[38−40] functionals with the Ahlrichs and co-workers' quadruple-ζ (def2-QZVP)[41,42] basis set with ECP for Mo and 6-311+G(2d,p)[43] basis set for all other atoms, referred to as BS2. Solvation effects were evaluated with SPEs using a self-consistent reaction field (SCRF) by treating the Et_2O solvent with the integral equation formalism variant of the polarizable continuum model (IEFPCM).[44] Natural bond orbital (NBO)[45] analysis was employed to evaluate the electron population on each element within required structures. In this paper, thermal-corrected Gibbs (ΔG) energies are reported at the M06/BS2//B3LYP/BS1 level of theory, unless otherwise noted. In addition, see Tables S1 and S2 in Supporting Information (SI) for validation of the DFT functional method.

The nomenclature used in this paper is as follows: (i) **N** (numbers) represent minima and **TS** represent intraconversion transition structures; (ii) spin-states are denoted by **S** (singlet), **D** (doublet), **T** (triplet), **Q** (quartet), and $\mathbf{Q_T}$ (quintet); (iii) breaking transition structures by **TSB**; (iv) the N[^{t}Bu]Ph ligand is represented by the **Ar** script; and (v) the N[^{t}Bu]Ph ligands are oriented in an almost C_{3V}, propeller-like arrangement, which has been reported as the most likely low-energy conformation.[20]

RESULTS AND DISCUSSION

Our investigation into the dual S═O bond activation and cleavage of a SO_2 molecule was performed by undertaking DFT calculations with MoL_3 (**1**), where L = NH_2 or N[^{t}Bu]Ph. The N[^{t}Bu]Ph ligand is more relevant to the experimental ligand (eq 1). The quartet $Mo(NH_2)_3$ (**1_Q**) is lower in energy than its doublet (**1_D**) by 58.2 kJ/mol, which is in accordance with earlier studies.[20,23,25,46−48] Consequently, the reaction pathway will begin along the quartet surface, as the ground state for SO_2 is a singlet. The earlier studies have revealed that there are two different conceivable approaches for bond cleavage within small molecules: mononuclear and binuclear mechanisms. We will examine both mechanisms in this study.

Scheme 1

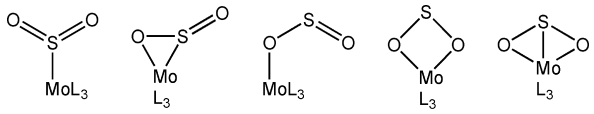

Coordination between SO_2 and $Mo(NH_2)_3$. The initial step is surmised to be SO_2 coordination onto **1_Q**, and there are five possibilities as shown in Scheme 1. Of these L_3Mo-SO_2 adducts, only three isomers were found to be stable along the quartet surface: η^1-S (**2_Q**), η^1-O (**4_Q**), and η^2-O,O (**5_Q**). As shown in Figure 1, **5_Q** is the most stable isomer (likely due to its η^2-binding mode) with a relative energy of −61.9 kJ/mol, while **2_Q** and **4_Q** have energies of −10.9 and −49.0 kJ/mol, respectively. Isomerization processes were also calculated between these three adducts, and results indicate that these intraconversions occur via small energy barriers (Figure 1).

The optimized geometries for the $(NH_2)_3Mo-SO_2$ minima along the quartet surface and free SO_2 are depicted in Figure 2. Interestingly, the SO_2 ligand in **2_Q** adopts a pyramidal geometry with respect to the Mo−SO_2 subunit, suggesting that SO_2 acts only as an electron acceptor in its interaction with the Mo metal center (for illustration see Figure S1 in Supporting Information).[5] For both **4_Q** and **5_Q**, the initial activation of the SO_2 is apparent as judged from S−O bond lengthening in their geometries as compared to that in free SO_2 (Figure 2). Since the analogous $Mo(NH_2)_3$ complexes, such as η^1-C-CO_2,[23] η^2-N,O-N_2O,[49] and η^2-C,S-CS_2,[25] are reported to be more stable as doublets rather than quartets, we have also examined the stabilities of $(NH_2)_3Mo-SO_2$ adducts along the doublet surface.

Intersystem crossing of **2_Q**, **4_Q**, and **5_Q** into their corresponding doublets can occur at minimum energy crossing points (MECPs), which were identified using the method of Harvey et al.[36] All of these spin-crossovers (quartet → doublet) are calculated to be energetically very small (Figure 1). Interestingly, for **4**, both spin-states are almost identical in relative energies, while **2** and **5** have doublets that are substantially more stable than their relevant quartets.

Along the doublet surface, two additional isomers were also found to be stable: η^2-S,O (**3_D**) and η^3-SO_2 (**6_D**) (Figure 1). Of all the $(NH_2)_3Mo$-SO_2 adducts, **3_D** is the most stable with a relative energy at −110.0 kJ/mol followed by **5_D** and **6_D** at −108.4 and −94.1 kJ/mol, respectively. The intraconversions from less stable isomers into **3_D** or **5_D** (resting-states) are calculated to have quite small barriers (Figure 1).

The optimized geometries for the $(NH_2)_3Mo$-SO_2 minima along the doublet surface and free SO (triplet-state) are depicted in Figure 3. Unlike **2_Q**, the **2_D** isomer adopts a planar SO_2 geometry, indicating that in addition to π-backbonding, the lone pair on the sulfur atom interacts with the empty orbital on the Mo center (Figure S1 in Supporting Information).[5] For **3_D**, the SO_2 ligand binds in a η^2-fashion, where its LUMO is oriented so that both sulfur and oxygen atoms accept electrons from the Mo metal center (Figure S1 in Supporting Information).[5]

The S−O bond lengths in **3_D** and **5_D** (1.726 and 1.668 Å, respectively) are even more elongated than those in **4_Q** and **5_Q**. This result indicates that the SO_2 activation on the doublet surface is more pronounced than that on the quartet surface. This is also supported by NBO population analysis; e.g., total SO_2 population for **5_D** (−0.661e) is calculated to be larger than that for **5_Q** (−0.416e).

Comparison with Analogous $Mo(NH_2)_3$ Studies. The $(NH_2)_3Mo-SO_2$ adducts are reasonably stable along the quartet surface, while previously reported adducts, such as $(NH_2)_3Mo-CO_2$[23] and $(NH_2)_3Mo-N_2$,[47,50] are not adequately stable on this surface. Intriguingly, in the SO_2 case, one electron is formally transferred from the Mo 4d-orbital into the SO_2 LUMO leading to metal oxidation ($Mo^{III} \rightarrow Mo^{IV}$) and weakening of the SO_2 π-bond. As shown in Table 1, this is supported by the fact that the calculated spin-density on the Mo metal center decreases from 3.14e in **1_Q** to 2.03e and 1.87e in **4_Q** and **5_Q**, respectively. Simultaneously, the SO_2 spin-density increases from 0.00e in free SO_2 to 1.03e and 1.00e

DOI: 10.1021/ic502298j
Inorg. Chem. 2015, 54, 534−543

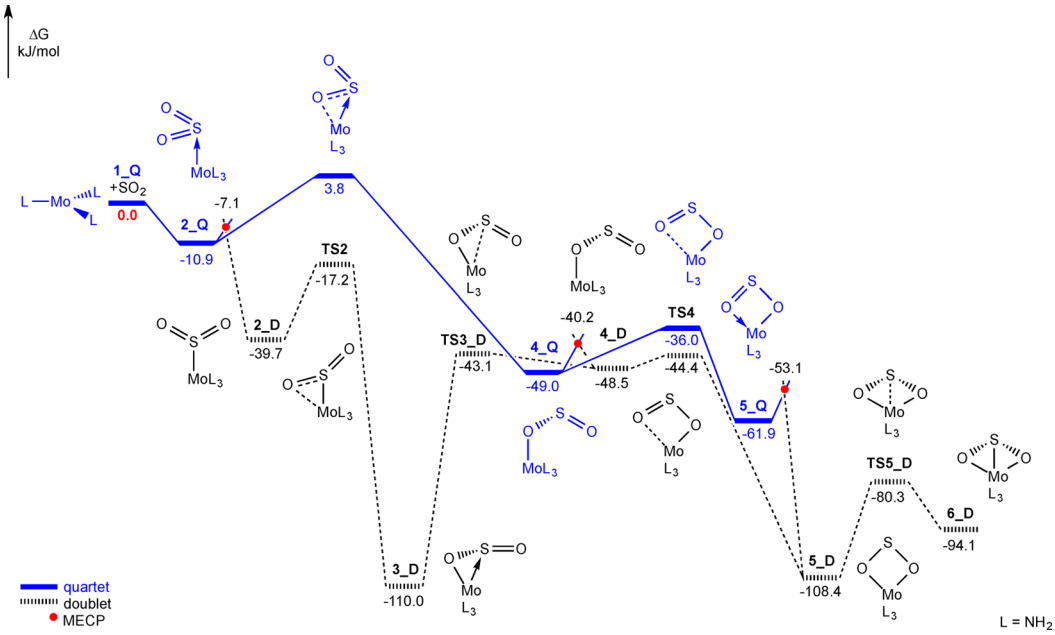

Figure 1. Energy profile for the SO_2 coordination onto $Mo(NH_2)_3$ (**1_Q**) along the quartet (blue/solid line) and doublet (black/dashed line) surfaces. MECPs are denoted by red dots. The thermal-corrected Gibbs (ΔG) energies are obtained at the M06/BS2//B3LYP/BS1 level in Et_2O. All energies are relative to **1_Q** and free SO_2 and given in kJ/mol.

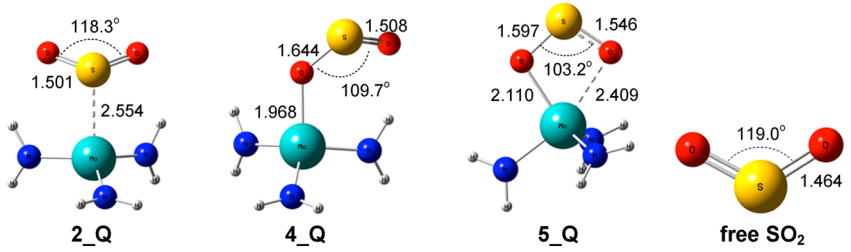

Figure 2. Optimized geometries of the $(NH_2)_3Mo\text{-}SO_2$ minima along the quartet surface (**Q**) and free SO_2 at the B3LYP/BS1 level. Selected bond lengths are in angstroms (Å), and bond angles are in degrees (°).

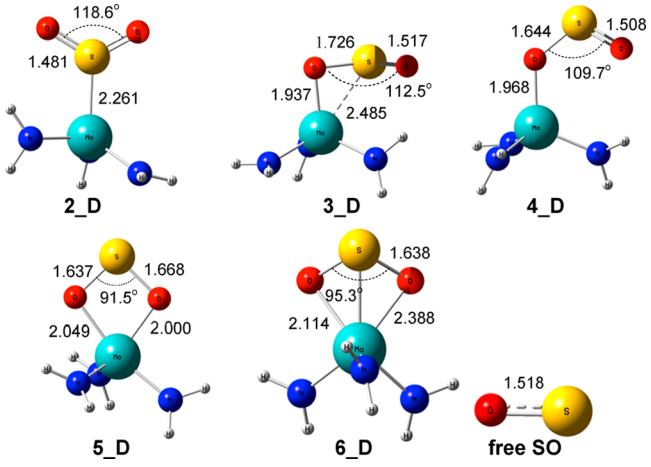

Figure 3. Optimized geometries of the $(NH_2)_3Mo\text{-}SO_2$ minima along the doublet surface (**D**) and free SO (triplet-state) at the B3LYP/BS1 level. Selected bond lengths are in angstroms (Å) and bond angles are in degrees (°).

in **4_Q** and **5_Q**, respectively. This electron transfer opens a vacant coordination site on Mo that allows optimal interaction between **1_Q** and SO_2, thus leading to stable $L_3Mo\text{-}SO_2$ adducts along the quartet surface. Interestingly, this electron transfer process was not observed for any of the other small molecules that we have previously studied,[23,25,47,49,50] and it appears to be a characteristic of this SO_2 system alone.

Table 1. Total Spin-Densities for the $(NH_2)_3Mo\text{–}SO_2$ Complexes[a]

	$Mo(NH_2)_3$	SO_2
1_Q	3.00	
2_Q	2.31	0.69
4_Q	1.97	1.03
5_Q	2.00	1.00
4AF	1.92	−0.92
5AF	1.86	−0.86
1_D	1.00	
2_D	1.05	−0.05
3_D	0.99	0.01
4_D	0.07	0.93
5_D	1.14	−0.14
6_D	0.82	0.18

[a]Obtained at the M06/BS2//B3LYP/BS1 level.

A qualitative evaluation of molecular orbitals allows us to understand the differences in stabilities of $Mo(NH_2)_3$ adducts. The molecular orbital interactions between **1_Q** and either SO_2 or CO_2 are schematically illustrated in Figure 4. For SO_2, the

DOI: 10.1021/ic502298j
Inorg. Chem. 2015, 54, 534−543

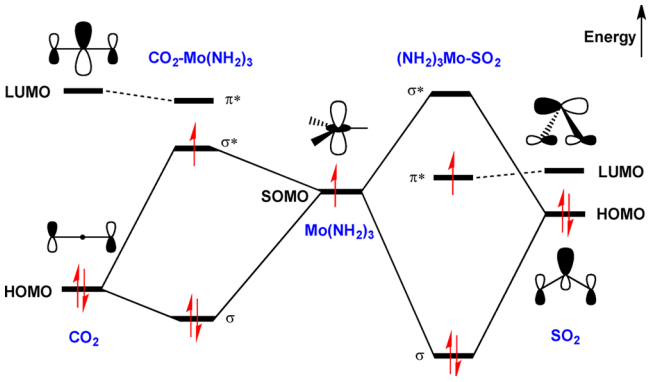

Figure 4. Simplified molecular orbital diagram for the interactions of $Mo(NH_2)_3$ (**1_Q**) with both SO_2 and CO_2[23] molecules.

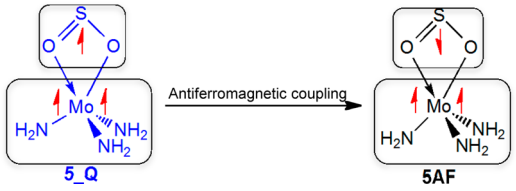

Figure 5. Illustration of antiferromagnetic (**AF**) coupling within $(NH_2)_3Mo(\eta^2\text{-}O,O\text{-}SO_2)$ (**5_Q**).

higher-lying HOMO leads to a strong interaction with **1_Q** and causes the Mo−SO_2 σ^*-orbital to lie above the lower-lying SO_2 π^*-orbital. In this case, the single electron occupies the π^*-antibonding orbital that assists in further stabilization of the $(NH_2)_3Mo-SO_2$ adduct. In contrast, the lower-lying HOMO of CO_2 leads to a weak interaction with **1_Q** and causes the Mo−CO_2 σ^*-orbital to lie below the higher-lying CO_2 π^*-orbital. In this case, the single electron occupies the σ^*-antibonding orbital leading to destabilization of the $(NH_2)_3Mo-CO_2$ adduct.[23] From this analysis, it can be concluded that triatomic molecules with lower-lying LUMOs and higher-lying HOMOs have a greater affinity for binding with MoL_3 along the quartet surface (for further details of small molecule orbitals; see Figure S2 in Supporting Information).

Both **4_Q** and **5_Q** have two unpaired electrons on the Mo metal center and one unpaired electron on the SO_2 ligand, as previously mentioned. Remarkably, this characteristic allows for ferromagnetic coupling between $Mo(NH_2)_3$ and SO_2 fragments, as shown in Figure 5. When an electron undergoes a spin-flip, namely, on the SO_2 ligand, pseudo doublet-state structures are achieved with different electronic configurations to that of **4_Q** and **5_Q** (Table 1), yet with identical geometric parameters. These resulting doublet-like structures will have antiferromagnetic (AF) coupling properties. With this AF nature, the relative energies of **4_Q** and **5_Q** are further

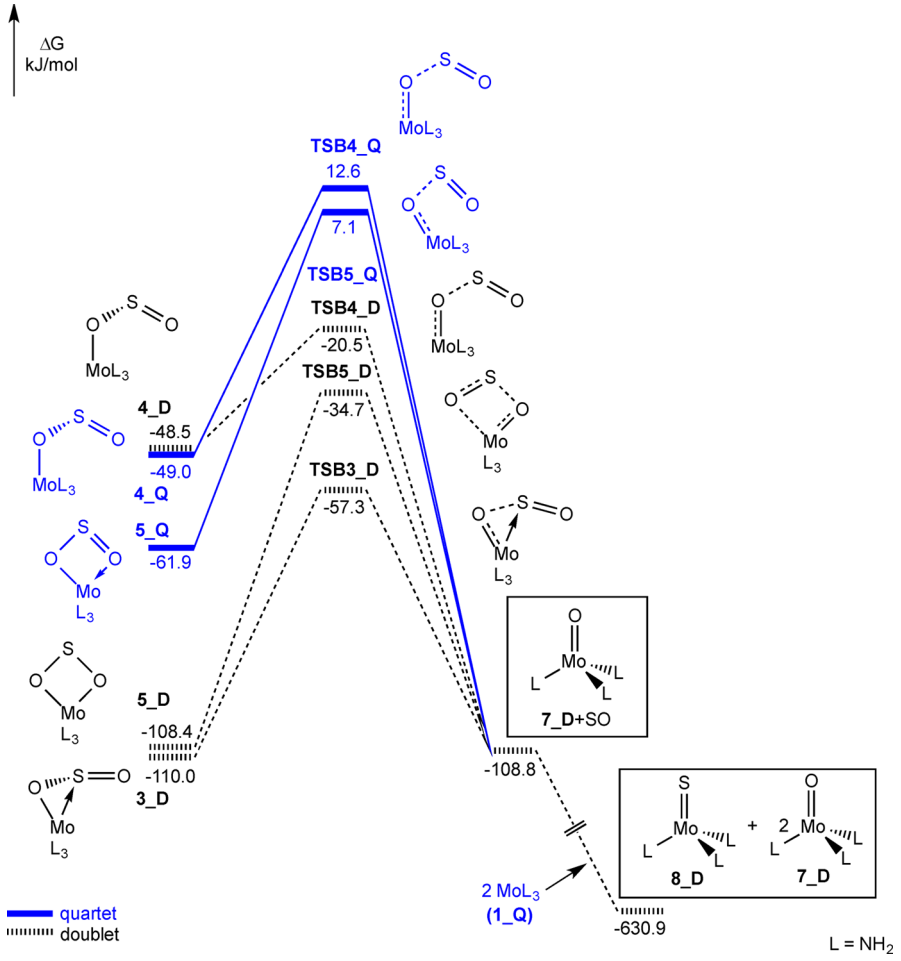

Figure 6. Energy profile for the dual S=O bond breaking with 1 equiv of $Mo(NH_2)_3$ (**1_Q**) along the quartet (blue/solid line) and doublet (black/dashed line) surfaces. The thermal-corrected Gibbs (ΔG) energies are obtained at the M06/BS2//B3LYP/BS1 level in Et_2O. All energies are relative to **1_Q** and free SO_2 in Figure 1 and are given in kJ/mol.

DOI: 10.1021/ic502298j
Inorg. Chem. 2015, 54, 534−543

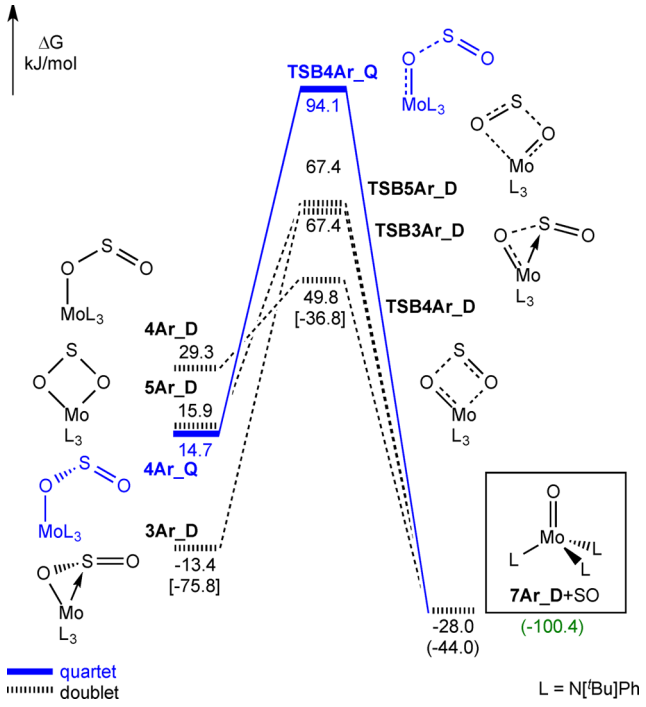

Figure 7. Energy profile for S═O bond breaking with 1 equiv of $Mo(N[^tBu]Ph)_3$ (**1Ar_Q**) along the quartet (blue/solid line) and doublet (black/dashed line) surfaces. All thermal-corrected Gibbs (ΔG) and enthalpy (ΔH) energies are obtained at the M06/BS2//B3LYP/BS1 level in Et_2O. The ΔH energies are shown in parentheses: experimental[17] (green) and calculated (black) values. Energies for ΔG at the B3LYP-D3BJ/BS2//B3LYP/BS1 level are shown in brackets (for complete B3LYP-D3BJ energy profile see Figure S3 in Supporting Information). All energies are relative to **1Ar_Q** and free SO_2 and are given in kJ/mol.

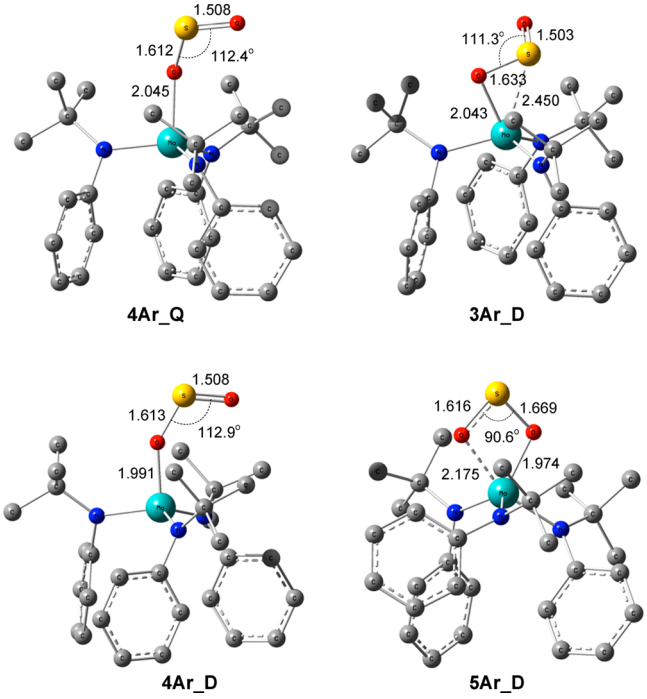

Figure 8. Optimized geometries of $(N[^tBu]Ph)_3Mo{-}SO_2$ minima at the B3LYP/BS1 level. Selected bond lengths are in angstroms (Å), and bond angles are in degrees (°). All hydrogen atoms omitted for clarity.

stabilized by 2.7 and 17.8 kJ/mol, respectively. However, this AF coupling between the Mo and SO_2 is completely quenched along the doublet surface. As a result, AF is more likely responsible for driving intersystem crossings.

Mononuclear Pathway for Initial S═O Breaking. By reacting SO_2 with 1 equiv of $Mo(N[R]Ar)_3$ (R = $C(CD_3)_2CH_3$, Ar = 3,5-$C_6H_3Me_2$), the product formation of $(N[R]Ar)_3Mo(O)$ was confirmed by ^2H NMR spectroscopy (δ = 7.41).[17] Thus, it is surmised that after SO_2 coordination onto the Mo metal center the next step is direct S═O bond cleavage, as shown in Figure 6. Even though **4_Q** and **5_Q** are capable of undergoing the S═O cleavage reaction, their breaking transition structures (**TSB4_Q** and **TSB5_Q**) lie above all the doublet breaking transition structures. This result suggests that the S═O cleavage is impossible to initiate from a quartet structure and must instead happen along the doublet surface. Efforts to locate a breaking transition structure from **6_D** only led to formation of **TSB5_D**. Furthermore, the relative energies of **TSB4_D** and **TSB5_D** lie above that of **TSB3_D** and indicate that initial S═O breaking should more likely occur from **3_D**.

The SO_2 ligand is more activated in **3_D**, and this is evident from a longer S−O bond distance as compared to that in other isomers (Figures 2 and 3). Indeed, simultaneous interaction of sulfur and an oxygen atom with Mo provides an optimal condition for SO_2 activation in **3_D**. In the other $(NH_2)_3Mo{-}SO_2$ adducts, this optimal interaction is not provided (see Figure S1 in Supporting Information), and therefore, the cleavage reaction requires a higher activation barrier. This result indicates that the S═O bond breaking is likely to occur from an isomer in which the SO_2 ligand is more activated. In addition, this cleavage reaction is calculated to be thermoneutral as the corresponding products, $(NH_2)_3Mo(O)$ (**7_D**) and SO, have a relative energy nearly identical to that of **3_D** (Figure 6).

Mononuclear Pathway with Bulkier System. The $N[^tBu]Ph$ (**Ar**) ligand was also investigated to determine how the addition of steric effects can influence SO_2 activation. Similar to that of the model system (L = NH_2), **3Ar_D** is calculated to be the resting state and is the only thermodynamically stable isomer in this bulkier system, as shown in Figure 7. All the other $N[^tBu]Ph$ isomers energetically lie above that of $Mo(N[^tBu]Ph)_3$ (**1Ar_Q**) and free SO_2. Attempts to locate **5Ar_Q** led to the formation of **4Ar_Q**.

The optimized geometries for the $(N[^tBu]Ph)_3Mo{-}SO_2$ minima are depicted in Figure 8. The lower stabilities of these $N[^tBu]Ph$ isomers are attributed to weak interactions between SO_2 and the Mo metal center. This is apparent as judged from the Mo−O bond lengthening within the bulkier system as compared to those in the model system (Figures 2 and 3). For example, the Mo−O bond distance in **3_D** is 1.937 Å, while that in **3Ar_D** is lengthened to 2.043 Å. This result indicates that there are substantial steric factors within **1Ar_Q** that lead to weakening of the $Mo{-}SO_2$ bond strength. In such a case, intraconversion processes between $N[^tBu]Ph$ isomers are expected to be facile and occur via SO_2 dissociation/association methods.

In contrast to the model system, the S═O cleavage reaction in the bulkier system is calculated to occur from the less sterically demanding **4Ar_D** isomer. In other words, **4Ar_D** with a η^1-binding mode is the best candidate for S═O bond breaking as **TSB4Ar_Q** lies below all the other breaking transition structures (Figure 7). In addition, the cleavage

DOI: 10.1021/ic502298j
Inorg. Chem. 2015, 54, 534−543

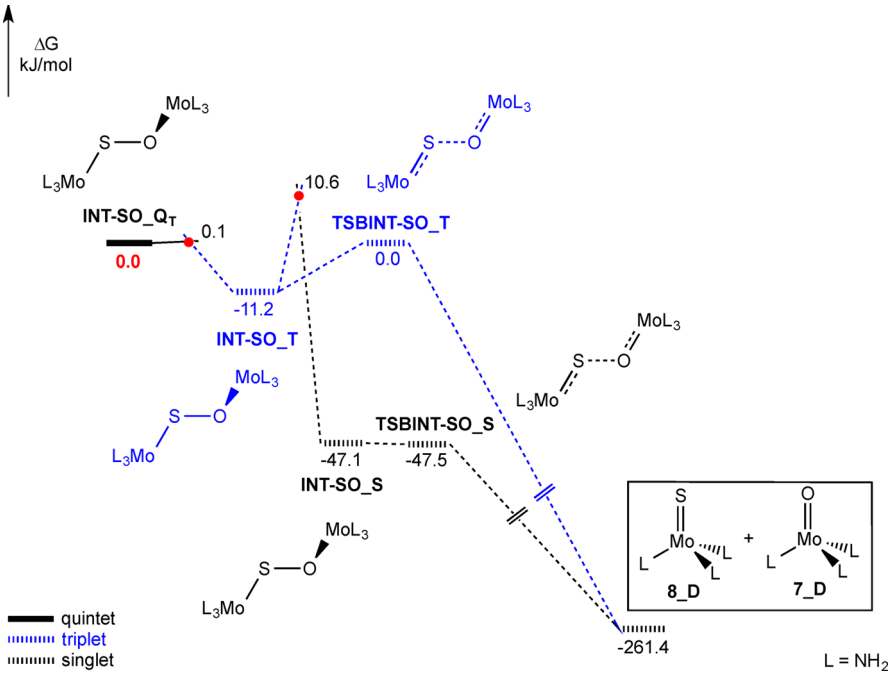

Figure 9. Energy profile for the second S═O bond cleavage with 2 equiv of $Mo(NH_2)_3$ (**1_Q**) and the resulting SO molecule. The thermal-corrected Gibbs (Δ*G*) energies are obtained at the M06/BS2//B3LYP/BS1 level in Et_2O. MECPs are denoted by red dots. All energies are relative to $(NH_2)_3Mo{-}S{-}O{-}Mo(NH_2)_3$ (**INT−SO_Q$_T$**) and given in kJ/mol.

reaction for the N[^{t}Bu]Ph ligand is calculated to be slightly exergonic, unlike the NH_2 ligand.

At this point, it is worth noting that the calculated enthalpy (Δ*H* = −44.0 kJ/mol, Figure 7) for the S═O cleavage reaction in the bulkier system is in disagreement with the experimental value (Δ*H* = −100.4 kJ/mol).[17] This is attributed to the limitations in incorporating long-range correlation for dispersion forces by density functional methods, such as the M06 functional.[52] Using Grimme's −D3 dispersion correction with Becke/Johnson-damping (B3LYP-D3BJ) functional,[51] single-point energies (SPEs) were calculated for all structures in Figure 7 to evaluate dispersion effects for the N[^{t}Bu]Ph ligands (for energy profile see Figure S2 in the Supporting Information). The difference between functionals leads to a significant increase in stabilities of all stationary points at the B3LYP-D3BJ level. All other trends are consistent with M06 results (Figure 7), except that **4Ar_D** → **TSB4Ar_D** is barrierless. The close agreement of the calculated enthalpy (Δ*H* = −118.5 kJ/mol) with the experimental value provides justification for the B3LYP-D3BJ energies.

The key outcome from this section is that unlike the model system (L = NH_2) in which electronic factors control the reactivity, steric factors appear to contribute an important role in controlling the reactivity of the bulkier system (L = N[^{t}Bu]Ph).

Breaking of the SO Molecule. The second S═O bond cleavage reaction proceeds through coordination of the two remaining **1_Q** species onto the resulting triplet SO molecule, which results from the oxygen abstraction by the first MoL_3. As shown in eq 2, it is surmised that the formation of the binuclear

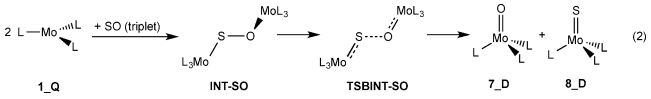

intermediate, $(NH_2)_3Mo{-}S{-}O{-}Mo(NH_2)_3$ (**INT−SO**), is a prerequisite for breaking of the SO molecule. After **INT−SO_Q$_T$** formation, the lowest-energy pathway is commenced by intersystem crossing (quintet → triplet) to form **INT−SO_T** followed by direct S−O bond breaking via **TSBINT−SO_T** (Figure 9). This leads to product formation of $(NH_2)_3Mo(S)$ (**8_D**) and another **7_D** complex, which is consistent with the experimental findings.[17] The entire reaction, 3 $Mo(NH_2)_3$ + SO_2 → 2 $(NH_2)_3Mo(O)$ + $(NH_2)_3Mo(S)$, is calculated to be strongly exergonic by −630.9 kJ/mol.

The breaking of the second S═O bond is calculated to be much faster (i.e., smaller activation barrier) than that of the first S═O bond. Therefore, the rate-determining step in the mononuclear mechanism for dual S═O bond cleavage should be the initial S═O breaking process.

Binuclear Pathway for Breaking of SO_2. Though the mononuclear mechanism is previously discussed, a binuclear mechanism is still feasible considering that 3 equiv of Mo(N[R]Ar) complexes are required for dual S═O bond cleavage (eq 1). The binuclear mechanism begins by coordination of **1_Q**/**1Ar_Q** onto the resting-state **3_D**/**3Ar_D**. For the bulkier system, the only geometry calculated to be stable along the quintet surface is the η^1-O//η^1-O isomer (**9Ar_Q$_T$**), depicted in Figure 10.

Herein, it is noteworthy to mention that **9Ar_Q$_T$** is the first example of a stable binuclear species located along the quintet surface. Other small molecules, such as N_2, CO_2, N_2O, and CS_2, are unstable on this surface and have not been previously reported.[23,25,47,49,50] The stability of **9Ar_Q$_T$** can be attributed to the low-lying π^*-orbital of SO_2. In this case, the second Mo coordination would formally transfer an electron via the SO_2 ligand into the first Mo metal and forces two electrons to reside on SO_2, resulting in an overall oxidation state of Mo^{IV}//Mo^{IV}. This is evident from spin-density analysis on the Mo metal

DOI: 10.1021/ic502298j
Inorg. Chem. 2015, 54, 534−543

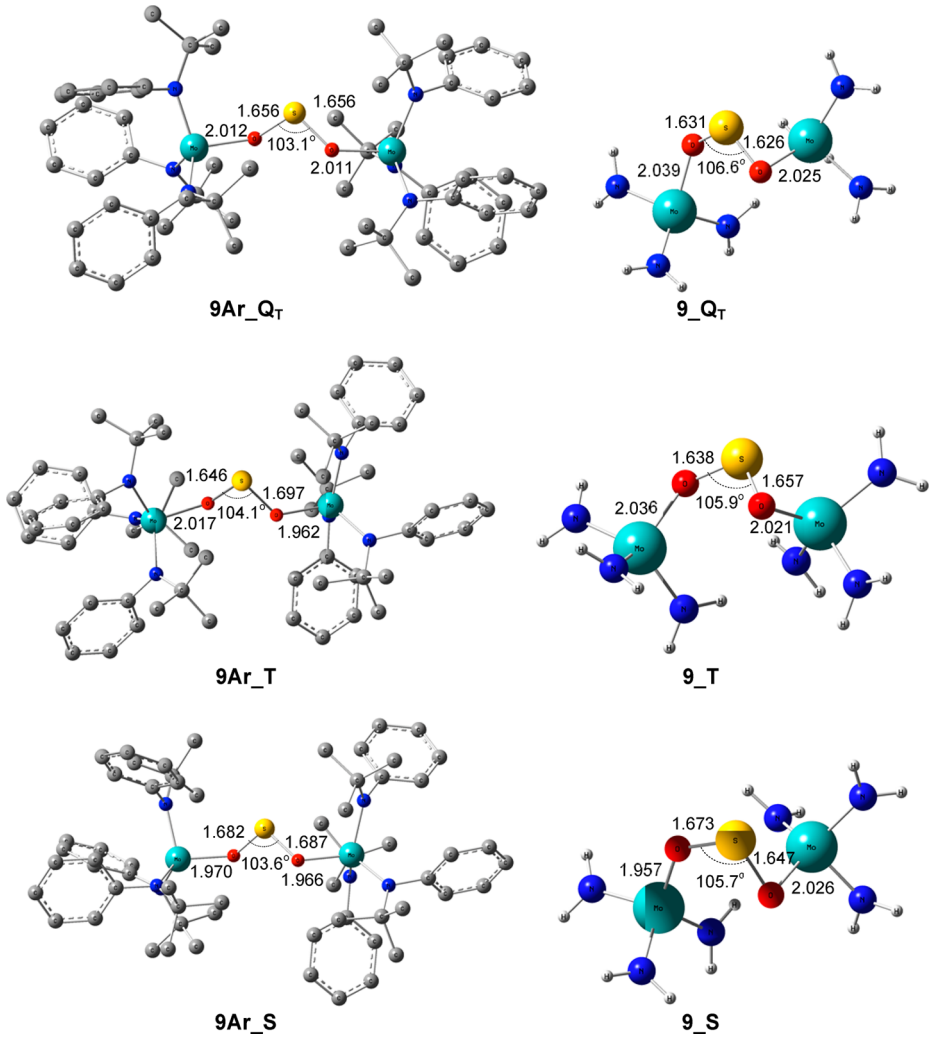

Figure 10. Optimized geometries of the binuclear minima at the B3LYP/BS1 level. Selected bond lengths are in angstroms (Å), and bond angles are in degrees (°). The N[^{t}Bu]Ph ligands are depicted without hydrogen atoms for clarity.

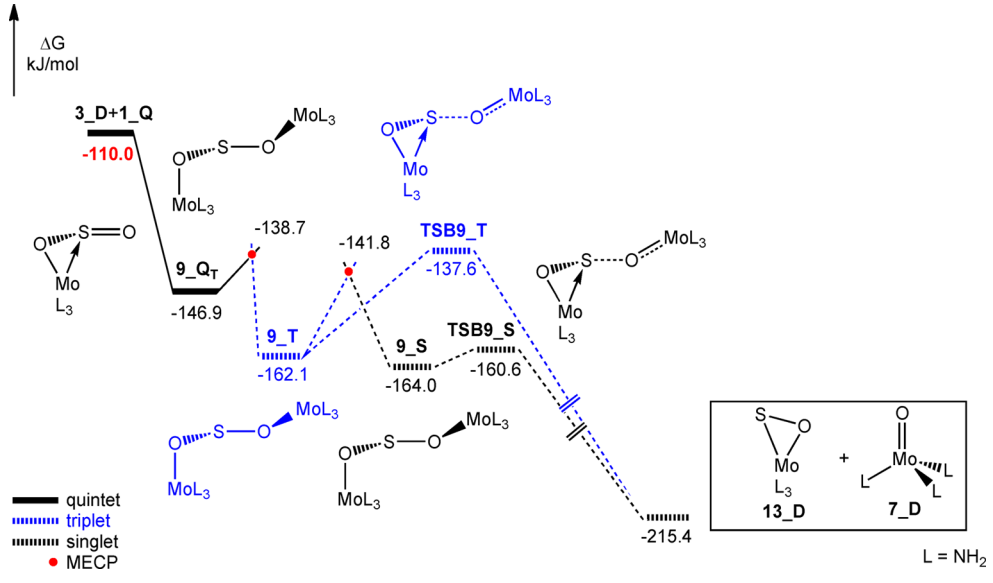

Figure 11. Energy profile of the binuclear mechanism for the S═O bond cleavage from $(NH_2)_3Mo(\eta^2\text{-S,O-}SO_2)$ (**3_D**) and $Mo(NH_2)_3$ (**1_Q**) along the quintet (black/solid line), triplet (blue/dashed line) and singlet (black/dashed line) surfaces. The thermal-corrected Gibbs (ΔG) energies are obtained at the M06/BS2//B3LYP/BS1 level in Et_2O. MECPs are denoted by red dots. All energies are relative to **1_Q** and free SO_2, as shown in Figure 1 and are given in kJ/mol.

DOI: 10.1021/ic502298j
Inorg. Chem. 2015, 54, 534−543

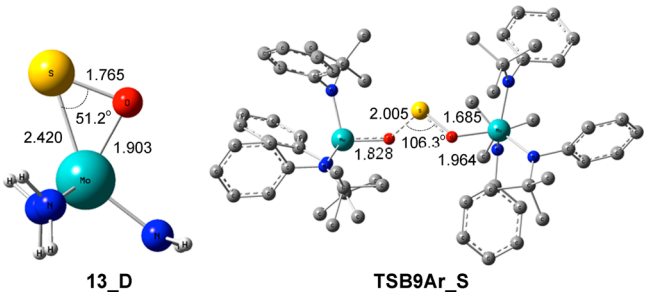

Figure 12. Optimized geometries of $(NH_2)_3Mo(\eta^2\text{-SO})$ (**13_D**) and the singlet bond breaking transition structure (**TSB9Ar_S**) at the B3LYP/BS1 level. Selected bond lengths are in angstroms (Å) and bond angles are in degrees (°). The N[^{t}Bu]Ph ligands are depicted without hydrogen atoms for clarity.

centers that are 1.86e//1.86e in **9Ar_Q$_T$**, while it is 3.14e in **1Ar_Q** and 1.01e in **3Ar_D**.

It is surmised that the next step is S═O bond cleavage, as shown in Figure 11. Initially, a simulated geometry of **9Ar_Q$_T$** using the NH_2 ligands, **9_Q$_T$**, was utilized to examine this process (Figure 10). In addition, the corresponding geometries of **9_T** and **9_S** were also simulated from **9Ar_T** and **9Ar_S**, respectively. From **9_Q$_T$**, the most favorable pathway for S═O bond breaking is calculated to initiate along the singlet surface (Figure 11). In this process, **9_Q$_T$** undergoes two consecutive intersystem crossings (quintet → triplet → singlet) to form **9_S** followed by the direct S−O bond cleavage via the breaking transition structure, **TSB9_S**. This binuclear process leads to product formation of **7_D** and $(NH_2)_3Mo(\eta^2\text{-SO})$ (**13_D**), depicted in Figure 12. Subsequently, the second S═O bond breaking occurs from **13_D** and the remaining **1_Q** via the process explained in Figure 9.

These results for the model system indicate that a binuclear mechanism is more favorable for dual S═O bond cleavage of SO_2. This also implies that the mononuclear mechanism is only preferred in the absence of excess $Mo(NH_2)_3$.

Binuclear Pathway with Bulkier System. The N[^{t}Bu]Ph ligand was also investigated to determine how the addition of steric effects can influence the binuclear mechanism. In contrast to that of the model system, all N[^{t}Bu]Ph isomers lie significantly higher in energy than that of **3Ar_D** + **1Ar_Q**, as shown in Figure 13. This instability is due to substantial increases in the steric interactions introduced by the second Mo metal center. The vital breaking transition structure for the S═O bond is via **TSB9Ar_S**, depicted in Figure 12. A comparison of Figures 7 and 13 reveals that **TSB4Ar_D** lies lower than that of **TSB9Ar_S**, indicating that for the bulkier system the mononuclear mechanism is the more favorable reaction pathway. This result is further supported by calculations at the B3LYP-D3BJ/BS2 level, shown in Figures 7 and 13.

CONCLUSION

Our theoretical investigation shows that 3 equiv of Mo(N[R]-Ar)$_3$ (R = $C(CD_3)_2CH_3$, Ar = 3,5-$C_6H_3Me_2$) is capable of undergoing dual S═O bond cleavage with a SO_2 molecule in the following sequence: (i) SO_2 coordination onto a MoL_3; (ii) oxygen abstraction by this MoL_3 (first bond cleavage) resulting in the formation of $L_3Mo{=}O$ and a SO molecule; and (iii) binding of two remaining MoL_3 onto the SO molecule leading to the second bond cleavage. This calculated mononuclear mechanism is in good agreement with the experimental findings reported by Cummins and co-workers.

Our results indicate that SO_2 coordination onto $Mo(NH_2)_3$ along the quartet surface is stronger than other di- or triatomic molecules, such as N_2, CS_2, CO_2, and N_2O. This is attributed to the lower-lying π^*-orbital of the SO_2 molecule which allows an electron to transfer from the Mo metal center onto the SO_2 ligand. This electron transfer leads to opening of an empty site

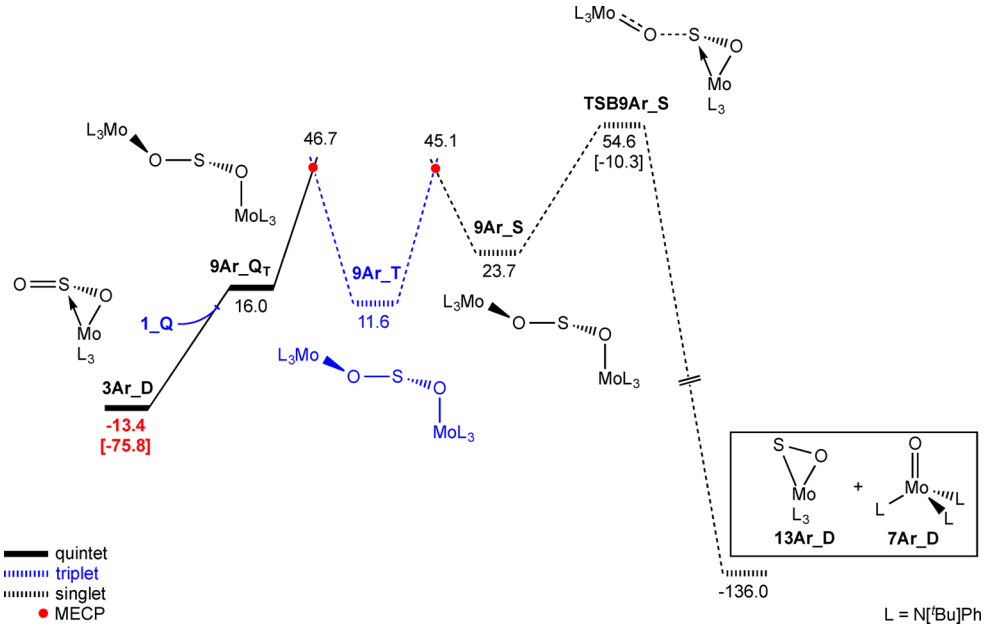

Figure 13. Energy profile of the binuclear mechanism for S═O bond cleavage from (N[^{t}Bu]Ph)$_3$Mo(η^2-S,O-SO_2) (**3Ar_D**) and Mo(N[^{t}Bu]Ph)$_3$ (**1Ar_Q**) along the quintet (black/solid line), triplet (blue/dashed line) and singlet (black/dashed line) surfaces. The thermal-corrected Gibbs (ΔG) energies are obtained at the M06/BS2//B3LYP/BS1 level in Et_2O. MECPs are denoted by red dots. Energies for ΔG values at the B3LYP-D3BJ/BS2//B3LYP/BS1 level are given in brackets. All energies are relative to **1Ar_Q** and free SO_2, as shown in Figure 7 and given in kJ/mol.

DOI: 10.1021/ic502298j
Inorg. Chem. 2015, 54, 534−543

on $Mo(NH_2)_3$, resulting in an optimum interaction between Mo and SO_2. Also due to this electron transfer, the $(NH_2)_3Mo-SO_2$ adducts were found to have antiferromagnetic (AF) coupling properties, which promotes intersystem crossing onto the doublet surface. The first S=O bond breaking reaction proceeds along the doublet surface after quenching the AF nature of these adducts.

In summary, the reactivity of the L_3Mo-SO_2 adducts toward SO_2 activation is generally influenced by the amide ligands (L = NH_2 or N[^{t}Bu]Ph). Within the model system, the reactivity is solely governed by electronic factors, whereas, for the bulkier system, steric factors contribute an important role in controlling the reactivity.

We have also investigated a prospective binuclear mechanism by which the dual S=O bond cleavage can occur. In contrast to that of other analogous species reported, a binuclear MoL_3 complex with SO_2 is reasonably stable along the quintet surface. This stability is attributed to the fact that SO_2 is capable of accepting two electrons from the Mo metal centers through its low-lying π^*-orbital. The binuclear mechanism proceeds in a related sequence to that of the mononuclear mechanism: (i) coordination of two MoL_3 onto SO_2; (ii) oxygen abstraction by a MoL_3 (first bond cleavage) resulting in $L_3Mo=O$ and $L_3Mo(SO)$; and (iii) binding of the remaining MoL_3 onto $L_3Mo(SO)$ for the second bond cleavage. Although for the model system the binuclear mechanism is more favorable, the higher instabilities of binuclear N[^{t}Bu]Ph isomers imply that the dual SO_2 cleavage with Mo(N[R]Ar) is most likely to occur via the mononuclear mechanism.

■ ASSOCIATED CONTENT

Supporting Information

Illustrations of molecular orbital interactions between SO_2 and the Mo metal. Diagram of frontier orbitals and their energies for common triatomic molecules. Validation of DFT functional methodology. Energy profiles for mononuclear S=O bond cleavage at the B3LYP-D3BJ/BS2//B3LYP/BS1 level in Et_2O. Cartesian coordinates and total energies for all optimized geometries, antiferromagnetic (AF) structures and minimum energy crossing points (MECPs). This material is available free of charge via the Internet at http://pubs.acs.org.

■ AUTHOR INFORMATION

Corresponding Authors

*E-mail: ariafard@yahoo.com (A.A.).
*E-mail: brian.yates@utas.edu.au (B.F.Y.).

Notes

The authors declare no competing financial interest.

■ ACKNOWLEDGMENTS

The authors thank the Australian Research Council (ARC) for financial project support (Grant DP120101937) and the Australian National Computational Infrastructure (NCI) and Tasmanian Partnership for Advanced Computing (TPAC) for provision of computing resources on the Raijin and Katabatic clusters. We also thank Prof. J. N. Harvey for providing the minimum energy crossing point (MECP) calculation code.

■ REFERENCES

(1) *The Clean Air Act of 1990*; United States Environmental Protection Agency (EPA); Government Printing Office: Washington, D.C., 1990.
(2) Rodriguez, J. A.; Liu, P.; Pérez, M.; Liu, G.; Hrbek, J. *J. Phys. Chem. A* **2009**, *114*, 3802.
(3) Rodriguez, J. A.; Jirsak, T.; González, L.; Evans, J.; Pérez, M.; Maiti, A. *J. Chem. Phys.* **2001**, *115*, 10914.
(4) Schenk, W. A. *Dalton Trans.* **2011**, *40*, 1209.
(5) Ryan, R. R.; Kubas, G. J.; Moody, D. C.; Eller, P. G. *Inorganic Chemistry*; Springer: Berlin Heidelberg, 1981; Vol. *46*, p 47.
(6) Kubas, G. J. *Acc. Chem. Res.* **1994**, *27*, 183.
(7) Laplaza, C. E.; Cummins, C. C. *Science* **1995**, *268*, 861.
(8) Laplaza, C. E.; Johnson, M. J. A.; Peters, J. C.; Odom, A. L.; Kim, E.; Cummins, C. C.; George, G. N.; Pickering, I. J. *J. Am. Chem. Soc.* **1996**, *118*, 8623.
(9) C. Cummins, C. *Chem. Commun.* **1998**, 1777.
(10) Peters, J. C.; Cherry, J.-P. F.; Thomas, J. C.; Baraldo, L.; Mindiola, D. J.; Davis, W. M.; Cummins, C. C. *J. Am. Chem. Soc.* **1999**, *121*, 10053.
(11) Gambarotta, S.; Scott, J. *Angew. Chem., Int. Ed.* **2004**, *43*, 5298.
(12) Laplaza, C. E.; Odom, A. L.; Davis, W. M.; Cummins, C. C.; Protasiewicz, J. D. *J. Am. Chem. Soc.* **1995**, *117*, 4999.
(13) Peters, J. C.; Baraldo, L. M.; Baker, T. A.; Johnson, A. R.; Cummins, C. C. *J. Organomet. Chem.* **1999**, *591*, 24.
(14) C. Peters, J.; L. Odom, A.; C. Cummins, C. *Chem. Commun.* **1997**, 1995.
(15) Greco, J. B.; Peters, J. C.; Baker, T. A.; Davis, W. M.; Cummins, C. C.; Wu, G. *J. Am. Chem. Soc.* **2001**, *123*, 5003.
(16) J. A. Johnson, M.; L. Odom, A.; C. Cummins, C. *Chem. Commun.* **1997**, 1523.
(17) Johnson, A. R.; Davis, W. M.; Cummins, C. C.; Serron, S.; Nolan, S. P.; Musaev, D. G.; Morokuma, K. *J. Am. Chem. Soc.* **1998**, *120*, 2071.
(18) Cherry, J.-P. F.; Johnson, A. R.; Baraldo, L. M.; Tsai, Y.-C.; Cummins, C. C.; Kryatov, S. V.; Rybak-Akimova, E. V.; Capps, K. B.; Hoff, C. D.; Haar, C. M.; Nolan, S. P. *J. Am. Chem. Soc.* **2001**, *123*, 7271.
(19) Cavigliasso, G.; Criddle, A.; Kim, H. S.; Stranger, R.; Yates, B. F. *Dalton Trans.* **2014**, *43*, 4631.
(20) Shaw, M. F.; Mahdizadeh Ghohe, N.; Ariafard, A.; Brookes, N. J.; Stranger, R.; Yates, B. F. *Dalton Trans.* **2014**, *43*, 1620.
(21) Cavigliasso, G.; Christian, G. J.; Stranger, R.; Yates, B. F. *Dalton Trans.* **2011**, *40*, 7327.
(22) Cavigliasso, G.; Wilson, L.; McAlpine, S.; Attar, M.; Stranger, R.; Yates, B. F. *Dalton Trans.* **2010**, *39*, 4529.
(23) Brookes, N. J.; Ariafard, A.; Stranger, R.; Yates, B. F. *Dalton Trans.* **2009**, 9266.
(24) Brookes, N. J.; Graham, D. C.; Christian, G.; Stranger, R.; Yates, B. F. *J. Comput. Chem.* **2009**, *30*, 2146.
(25) Ariafard, A.; Brookes, N. J.; Stranger, R.; Yates, B. F. *J. Am. Chem. Soc.* **2008**, *130*, 11928.
(26) Christian, G.; Stranger, R.; Yates, B. F.; Cummins, C. C. *Eur. J. Inorg. Chem.* **2007**, *2007*, 3736.
(27) For the full Gaussian09 reference, see the Supporting Information.
(28) Becke, A. D. *J. Chem. Phys.* **1993**, *98*, 5648.
(29) Lee, C.; Yang, W.; Parr, R. G. *Phys. Rev. B* **1988**, *37*, 785.
(30) Becke, A. D. *Phys. Rev. A* **1988**, *38*, 3098.
(31) Andrae, D.; Häußermann, U.; Dolg, M.; Stoll, H.; Preuß, H. *Theoret. Chim. Acta* **1990**, *77*, 123.
(32) Wiberg, K. B. *J. Comput. Chem.* **1986**, *7*, 379.
(33) Dennington, R.; Keith, T.; Millam, J. *GaussView5.0*; Semichem Inc.: Shawnee Mission, KS, 2009.
(34) Fukui, K. *Acc. Chem. Res.* **1981**, *14*, 363.
(35) Fukui, K. *J. Phys. Chem.* **1970**, *74*, 4161.
(36) Harvey, J. N.; Aschi, M.; Schwarz, H.; Koch, W. *Theor. Chem. Acc.* **1998**, *99*, 95.
(37) Grimme, S.; Ehrlich, S.; Goerigk, L. *J. Comput. Chem.* **2011**, *32*, 1456.
(38) Zhao, Y.; Truhlar, D. G. *J. Chem. Phys.* **2006**, *125*, 194101.
(39) Zhao, Y.; Truhlar, D. G. *J. Phys. Chem. A* **2006**, *110*, 13126.

DOI: 10.1021/ic502298j
Inorg. Chem. 2015, 54, 534−543

(40) Zhao, Y.; Schultz, N. E.; Truhlar, D. G. *J. Chem. Theory Comput.* **2006**, *2*, 364.
(41) Weigend, F.; Furche, F.; Ahlrichs, R. *J. Chem. Phys.* **2003**, *119*, 12753.
(42) Weigend, F.; Ahlrichs, R. *Phys. Chem. Chem. Phys.* **2005**, *7*, 3297.
(43) McLean, A. D.; Chandler, G. S. *J. Chem. Phys.* **1980**, *72*, 5639.
(44) Tomasi, J.; Mennucci, B.; Cammi, R. *Chem. Rev.* **2005**, *105*, 2999.
(45) Glendening, E. D.; Reed, A. E.; Carpenter, J. E.; Weinhold, F. *NBO ver.* 3.1; Gaussian Inc.; Pittsburgh, PA, 2003.
(46) Christian, G.; Stranger, R.; Yates, B. F.; Cummins, C. C. *Dalton Trans.* **2008**, 338.
(47) Neyman, K. M.; Nasluzov, V. A.; Hahn, J.; Landis, C. R.; Rösch, N. *Organometallics* **1997**, *16*, 995.
(48) Christian, G.; Stranger, R.; Petrie, S.; Yates, B. F.; Cummins, C. C. *Chem.—Eur. J.* **2007**, *13*, 4264.
(49) Khoroshun, D. V.; Musaev, D. G.; Morokuma, K. *Organometallics* **1999**, *18*, 5653.
(50) Hahn, J.; Nasluzov, V. A.; Neyman, K. M.; Rösch, N. *Inorg. Chem.* **1997**, *36*, 3947.
(51) Marom, N.; Tkatchenko, A.; Rossi, M.; Gobre, V. V.; Hod, O.; Scheffler, M.; Kronik, L. *J. Chem. Theory Comput.* **2011**, *7*, 3944.
(52) Grimme, S. *WIREs: Comput. Mol. Sci.* **2011**, *1*, 211.

DOI: 10.1021/ic502298j
Inorg. Chem. 2015, 54, 534−543